Multiscale Control of Hierarchical Structure in Crystalline Block Copolymer Nanoparticles Using Microfluidics

Aman Bains, Yimeng Cao, & Matthew G. Moffitt

August 2015

The final publication is available at:

https://doi.org/10.1002/marc.201500359

WILEY-VCH

DOI: 10.1002/marc.201500359
Article type: Communication

Multiscale Control of Hierarchical Structure in Crystalline Block Copolymer Nanoparticles using Microfluidics

*Aman Bains, Yimeng Cao, Matthew G. Moffitt**

Department of Chemistry, University of Victoria, P.O. Box 3065, Victoria, BC, Canada V8W 3V6

Keywords: Block Copolymers, Self-Assembly, Drug Delivery, Microfluidics, Nanoparticles

The solution self-assembly of amphiphilic block copolymers to form micellar nanoparticles has become one of the most broadly researched topics of colloidal nanoscience.[1] A growing number of potential applications, including drug delivery,[2] sensing,[3] and medical imaging,[4] highlights the need for methods of generating block copolymer nanoparticles with controlled structural parameters (e.g. size and shape). The vast majority of research efforts have applied variation in chemical conditions (e.g. copolymer composition, concentration, and solvent) to change the nature and strength of intermolecular forces and thus the structural products of self-assembly ("bottom-up" control).[1] More recently, a small number of studies have applied forces external to the molecular system (e.g. shear or confinement) to direct the structural outcome of self-assembly ("top-down" control);[5] such strategies offer the potential for "dialing in" specific nanostructures through simple changes in processing conditions without the need to alter chemical formulations. For example, recent work from our group has shown that localized high-shear "hot spots" within segmented gas-liquid microfluidic reactors enable flow-directed self-assembly of polystyrene-*block*-poly(acrylic acid) (PS-*b*-PAA), providing "top-down" control of nanoparticle morphologies and sizes *via* flow rate under constant chemical conditions.[6]

Micellar nanoparticles formed from semicrystalline block copolymers, including poly(L-lactide)-*block*-poly(ethylene oxide) (PLLA-*b*-PEO) and polycaprolactone-*block*-poly(ethylene oxide)(PCL-*b*-PEO), have recently garnered increased attention, due in part to the importance of such materials for drug delivery applications.[7] Such nanoparticles exhibit multiscale organization, or structural hierarchy, due to a combination of structural features at the colloidal length scale (~10-100 nm), characterized by the size and morphology of the nanoparticles, and at the nanoscale (~1-10 nm), characterized by the ordering of chain segments within crystallites in the nanoparticle cores. For drug delivery, organization on both of these disparate length scales is critical to the functions of selected targeting and drug release.[8,9] For example, nanoparticle size and morphology are found to strongly influence biodistribution (e.g. *via* the enhanced permeability and retention effect in tumours) and circulation time,[8] while internal crystallinity is a critical factor of particle stability, flexibility and release rate.[8,9]

The recent interest in microfluidics for preparing drug delivery nanoparticles has been spurred by the potential for fast and efficient on-chip screening and fine control of reagent concentrations.[10] However, a microfluidic approach offering continuous variability of structure on *both* critical length scales has not been previously demonstrated; such a platform would greatly enhance opportunities for tailoring nanomedicine function for specific treatments and optimum patient outcomes. In this paper, we apply a segmented microfluidic reactor to the generation of semicrystalline and biocompatible PCL-*b*-PEO micellar nanoparticles, demonstrating that structural features on multiple length scales, including nanoparticle sizes, morphologies and internal crystallinities, can be tuned *via* flow rate under constant chemical conditions. The application of unique flow fields[6] within the reactor to direct multiple levels of organization simultaneously through a single control variable highlights the general utility of this microfluidic reactor for the controlled manufacturing of hierarchical polymeric nanoparticles. Next, we demonstrate a proof-of-concept application of

the microfluidic platform to the production of PCL-*b*-PEO drug delivery nanoparticles containing the anti-cancer agent paclitaxel (PAX); we show that flow-directed control of multiscale structure enables optimization of PAX loading and top-down variability of drug release kinetics.

The specific polymer used in this work is PCL_{105}-*b*-PEO_{114}, where numbers in subscripts denote number-average degrees of polymerization for the respective blocks. The gas-liquid segmented microfluidic system (Figure 1) is described in our previous papers.[6] For all microfluidic and bulk (control) self-assembly experiments, the starting condition was 0.33 wt. % copolymer in *N*,*N*-dimethylformamide (DMF) with micellization induced by the addition of water above the critical water concentration (cwc = 5.5 wt %). Increasing the total flow rate (gas + liquid) increases linearly the maximum shear rate in the hot spots; therefore, multiple flow rates and water contents were investigated in order to vary both chemical and shear forces during self-assembly. For preliminary PAX loading experiments reported here, a drug : copolymer ratio of 0.01 (w/w) was employed.

Microfluidic self-assembly (Figure 1) was initiated by combining three liquid streams at the reactor inlet: 1.DMF/PCL-*b*-PEO (or DMF/PCL-*b*-PEO/PAX for drug loading), 2.DMF (separator stream), and 3.DMF/water. The streams were joined with argon gas, which compartmentalized the liquid plugs and induced chaotic advection, enabling fast mixing and triggering nanoparticles formation. PCL-*b*-PEO nanoparticles then proceeded through the processing channel where they were exposed to high shear hot spots. Unless otherwise stated, nanoparticles without PAX were collected from the reactor into empty vials for immediate characterization by transmission electron microscopy (TEM), x-ray powder diffraction (XRD) and differential scanning calorimetry (DSC); PAX-loaded PCL-*b*-PEO nanoparticles were collected into a 10x-excess volume of water and then dialyzed overnight to remove residual DMF and unencapsulated PAX, followed by characterization and release studies. For comparison with on-chip results, a conventional bulk PAX-loading experiment was carried

out in which water was added dropwise to the copolymer/PAX solution to 80 wt % followed by overnight dialysis.[2a]

We first investigated the on-chip self-assembly of PCL-*b*-PEO without PAX. Figure 2 shows TEM images of the plethora of nanoparticle morphologies obtained at three water contents (cwc + 2 wt %, cwc + 5 wt %, and cwc + 10 wt %) and four flow rates (5, 25, 50, and 100 μL/min) from a single PCL-*b*-PEO block copolymer. At each water content, all major nanoparticle morphologies— spheres, cylinders (filomicelles), lamellae and vesicles (polymersomes)— are formed on-chip by changing flow rate between 5 and 100 μL/min. This demonstrates top-down control of PCL-*b*-PEO morphologies *via* flow rate under constant chemical conditions. At each water content, the observed morphologies change non-monotonically, going through a minimum in interfacial curvature with increasing flow rate. For example, at cwc + 10 wt % (Figure 2, I-L), high-curvature spheres are generated at 5 μL/min, with lower-curvature cylinders and lamellae, and then vesicles, appearing as the flow rate increases to 25 and 50 μL/min, respectively; finally, high-curvature spheres reappear at 100 μL/min. Prominent morphologies and their mean dimensions for each set of conditions are reported in Table S1 with excellent reproducibility observed over multiple preparations (Figures S2-S4).

These flow-directed morphologies reflect a complex interplay of chemical and shear forces operating in the channels. Similar to PS-*b*-PAA self-assembly within an identical reactor,[6] shear-induced coalescence and breakup mechanisms are expected to strongly influence morphologies formed on-chip. As described in our previous publications,[6] the vast majority of nanoparticles (~98% v/v) form outside the highly localized, high-shear hot spots. Following their initial formation upon mixing with water near the injector, nanoparticles circulate through the hot spots where high shear can increase the rate of coalescence, leading to larger, nonequilibrium aggregates; due to kinetic contraints, these aggregates relax via intramicellar rearragements to form various nonergotic morphologies. Another possibility

worthy of consideration is that under certain conditions the directionality of shear forces may facilitate the formation of cylinders via one-dimensional assembly of spheres[11] along the direction of shear; however, we point out that the formation of lamellae and vesicles under certain chemical and shear conditions indicates that such shear-templated one-dimensional assembly is not operative in all cases.

Crystallization of PCL blocks has been shown to have a strong effect on PCL-*b*-PEO morphologies,[7,12] and so the occurrence of flow-induced crystallization could also contribute to the observed flow dependence. Although flow-induced polymer crystallization from melt and solution states has been widely studied,[13] flow effects on block copolymer crystallization during solution self-assembly and nanoparticle formation have not been previously reported to our knowledge. XRD data for PCL-*b*-PEO nanoparticles collected at different flow rates show identical sharp reflections, suggesting flow rate does not affect the crystalline PCL and PEO unit cells (Figure S8); however, the incoherent scattering halo decreases markedly with increasing flow rate. To quantify this effect, PCL crystalline, PEO crystalline, and amorphous contributions were deconvoluted from XRD data and resulting peak areas were used to calculate percentages of crystalline PCL and PEO relative to the total copolymer mass (Figure 3, cwc + 10 wt %). The percentage of crystalline PEO shows no significant flow rate dependence, since PEO blocks are solubilized on-chip and crystallize during solvent evaporation after collection. In contrast, PCL crystallinity shows a marked linear dependence on flow rate, suggesting flow-induced crystallization within the hydrophobic nanoparticle cores. Total copolymer crystallinities from XRD and DSC give good agreement for the two methods (Figure 3). For the two lower on-chip water contents (cwc + 5 wt % and cwc + 2 wt %), similar linear increases in PCL crystallinity with increasing flow rate were obtained, with the slopes of the resulting plots decreasing with decreasing water content (Figure S8).

To understand the increase in internal nanoparticle crystallinity with increasing flow rate, we consider two related and well-studied phenomena: flow-induced cystallization of

polymers from solution and flow-induced crystallization of polymers from the melt state.[13] Polymer crystallization from solution is induced primarily by extensional components of flow (and not by shear), whereas shear components are found to induce polymer crystallization from the melt state.[13] For the present case, we consider that PCL blocks begin in the solution state, but upon mixing with water are transferred *via* self-assembly to the melt state within the nanoparticle cores. As indicated above, almost all high-shear exposure occurs after nanoparticle formation has taken place, such that flow-induced PCL crystallization should most closely ressemble the shear dependence of polymer crystallization from the melt state. This explains why increasing the maximum shear rate within the hot spots by increasing the flow rate increases the internal crystallinity of the micellar nanoparticles. Although we do not know the exact mechanism by which shear affects PCL crystallinity, we propose that transient and elastic nanoparticle deformations within the hot spots could result in elongation of internal PCL chains along the shear direction thus promoting nucleation of crystallites.

A particularly intriguing feature of these results is the contrast between the monotonic and linear increase in PCL crystallinity with increasing flow rate at all water contents and the corresponding non-monotonic changes in internal nanoparticle curvature. For quiescent self-assembly of PCL-*b*-PEO in aqueous media, nanoparticle morphologies are found to be strongly coupled to PCL crystallinity.[7,12] For example, Du et al. have demonstrated a strong correspondence between PCL-*b*-PEO nanoparticle morphologies and PCL crystallization temperatures;[12a] in addition, Eisenberg and coworkers have described crystallinity-driven transitions from spheres to rods on time scales from hours to weeks and from rods to ribbons and small lamellae on time scales of weeks to months.[12b] Both of these studies suggest that PCL crystallization favours particle morphologies with low internal curvature such as rods and platelets (lamellae). In contrast, our results demonstrate that in the unique flow environment of the reactor, morphology and crystallinity can be partly decoupled, due to additional and independent flow-directed mechanisms operating simultaneously with PCL

crystallization (e.g. particle breakup). As a result, on-chip combinations of multiscale structural features are generated at high flow rate (e.g. highly crystalline spheres generated at cwc + 10 wt % and 100 μL/min, Figure 2L and Figure 3) that would not normally form under bulk self-assembly conditions.

We next demonstrated the applicability of on-chip multiscale structure control to tailoring function for drug delivery, by preparing PAX-loaded PCL-*b*-PEO nanoparticles on-chip at cwc + 5 wt % and three different flow rates (25, 50, and 100 μL/min), and *via* conventional (bulk) dropwise water addition. Similar to nanoparticles without PAX, drug-loaded nanocarriers show flow-tunable morphologies and sizes, starting with spheres, and then filomicelles, and then filomicelles and lamellae, as flow rate increases (Figure 4A, Table S2), with a corresponding increase in mean effective hydrodynamic diameters from 47 to 1030 nm by dynamic light scattering (DLS, Figure S9). The PAX-loaded filomicelles, "dialed-in" *via* flow rate under constant chemical conditions, are particularly intriguing, due to demonstrated advantages over spheres of these flexible, fragmentable, and longer-circulating drug delivery vehicles.[8] Next, the structure and dynamics of the PAX-loaded nanoparticle cores were investigated, with XRD indicating an increase in core crystallinity with flow rate (Figure 4B, "zero-flow" represents bulk-prepared nanoparticles). The flow-dependence of the core environment was corroborated by fluorescence anisotropy of a hydrophobic probe (DPH) dissolved in the core. The increase in fluorescence anisotropy with flow rate indicates that as PCL crystallinity increases, so too does the microviscosity within the core (Figure 4B).[9a] Thus flow rate provides simultaneous multiscale control of the size and shape of polymer nanocarriers, as well as the internal diffusion environment of their hydrophobic cargo.

Finally, loading and release properties of the PAX-loaded nanoparticles were studied using high performance liquid chromatography-mass spectrometry (HPLC-MS) for PAX quantification (Figure 5). PAX loading efficiencies, defined as: loading efficiency(%) = [PAX

in nanoparticles(g)/total PAX used(g)] x 100%, show marked improvements with increasing flow rate, with an on-chip loading efficiency of ~90% at 100 μL/min compared to ~45% for the bulk-prepared control (Figure 5A). We attribute the increase in loading efficiency with flow rate to the corresponding evolution of filomicelles and lamellae from significantly smaller spheres (Figure 4A), since polymer nanoparticles with higher aggregation numbers generally lead to higher solubilities of hydrophobic drugs.[2f,8d] On the other hand, the increase in PCL crystallinity with flow rate (Figure 4B) should impede PAX encapsulation and so is not expected to contribute positively to the increased drug loading.

In vitro release profiles of PAX-loaded PCL-*b*-PEO nanoparticles under model physiological conditions (37 °C, PBS buffer: pH = 7.4, 45 g/L albumin) show slower release for all on-chip samples compared to the bulk-prepared sample (Figure 5B). Moreover, we find that on-chip flow rate provides a direct handle on release times. For the bulk-prepared nanocarriers, PAX is completely released after ~1 day; in contrast, for the 25 μL/min and 50 μL/min on-chip samples, complete release occurs over a total of ~5 and ~9 days, respectively. Finally, for the 100 μL/min sample, PAX release plateaus at ~85% after ~5 days, suggesting the remaining ~15% PAX is "trapped" in the higher-crystallinity cores (Figure 4B) formed at this flow rate. We note that such "dial-in" control of release times offers immense potential for tunable timed release of specific drugs for desired treatments. Flow-controlled PAX release times can be explained by the corresponding flow dependence of multiscale nanoparticle structure. As flow rate increases, both the core size (Figure 4A) and crystallinity (Figure 4B) increase; the corresponding increase in diffusion distance and decrease in diffusion coefficient, respectively, will both contribute to the observed increase in release time. Another consideration is that the effects of morphology and crystallinity on nanoparticle hydrolytic degradation (Figures S11-S15) may contribute to further flow dependences of drug release.[14]

We note that on the basis of simple diffusion and assuming equivalent PAX distributions within the cores, the significantly faster release time for the bulk sample compared to the on-chip 25 μL/min sample is not consistent with their relative nanoparticle sizes and crystallinities; this suggests an additional factor distinguishing PAX-loaded nanoparticles prepared on-chip from those prepared in the bulk. One possibility is that faster mixing (~1 s) within the reactor results in a more uniform distribution of PAX throughout the PCL cores, whereas relatively slow water addition during bulk preparations (including dropwise or dialysis addition)[2a] allows PAX to migrate to the core-coronae interface, significantly accelerating its release.

In summary, semicrystalline PCL-*b*-PEO nanoparticles were produced in a segmented gas-liquid microfluidic reactor with unprecedented top-down control of disparate levels of multiscale structural features, including nanoparticle morphologies, sizes, and internal crystallinities. Using the same microfluidic platform, PAX-loaded PCL-*b*-PEO nanoparticles were also produced with improved PAX loading efficiencies (up to 90%) and slower *in vitro* release kinetics compared to a conventional bulk preparation. Control of multiscale structure enabled tailoring of drug delivery nanoparticle function, as demonstrated by tuning of PAX release rates *via* on-chip flow rate. Investigations of the therapeutic applications of flow-directed polymeric nanocarriers, including cell viability studies, are currently underway in our lab.

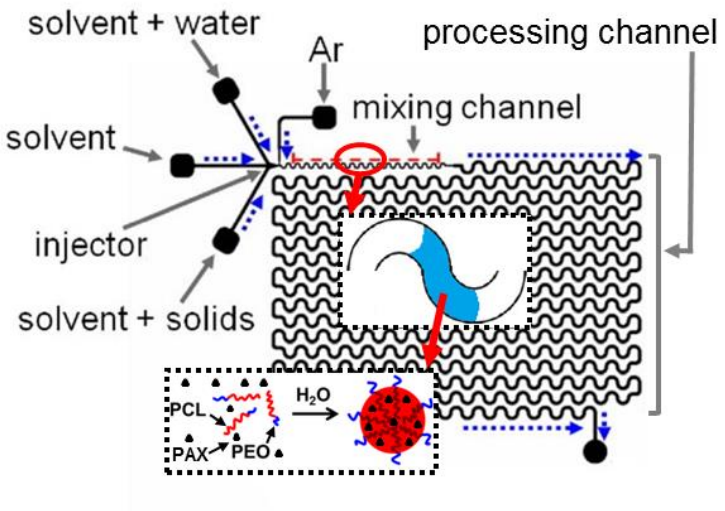

Figure 1. Schematic of the gas-liquid segmented reactor and on-chip formation of PAX-loaded PCL-*b*-PEO nanoparticles.

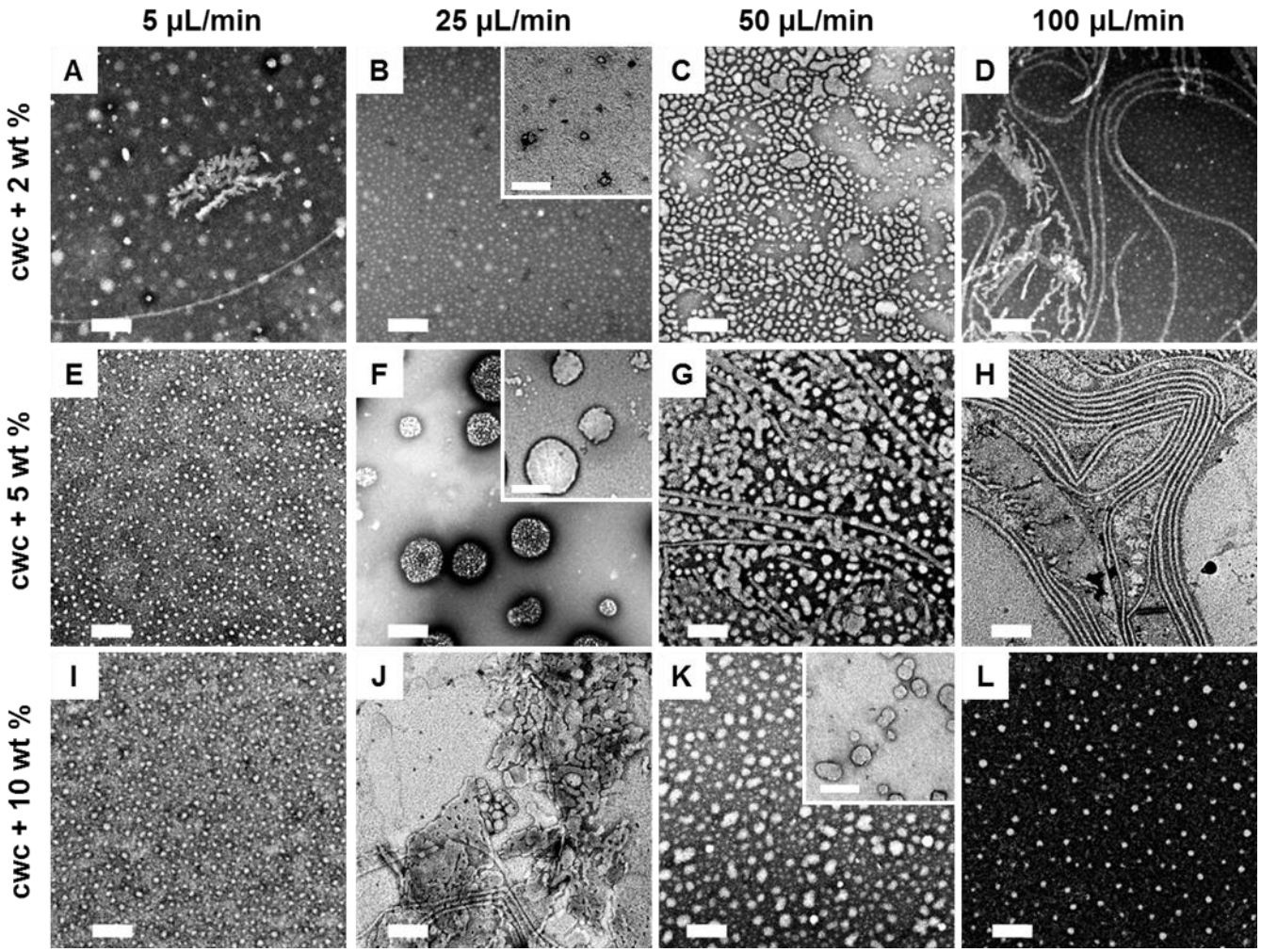

Figure 2. TEM images of multiple flow-directed morphologies of PCL-*b*-PEO nanoparticles formed on-chip at various water contents and flow rates. Main images were produced with negative staining with uranyl acetate; insets are unstained images allowing visualization of the internal lumen of vesicles. Main image scale bars are 200 nm and inset scale bars are 100 nm.

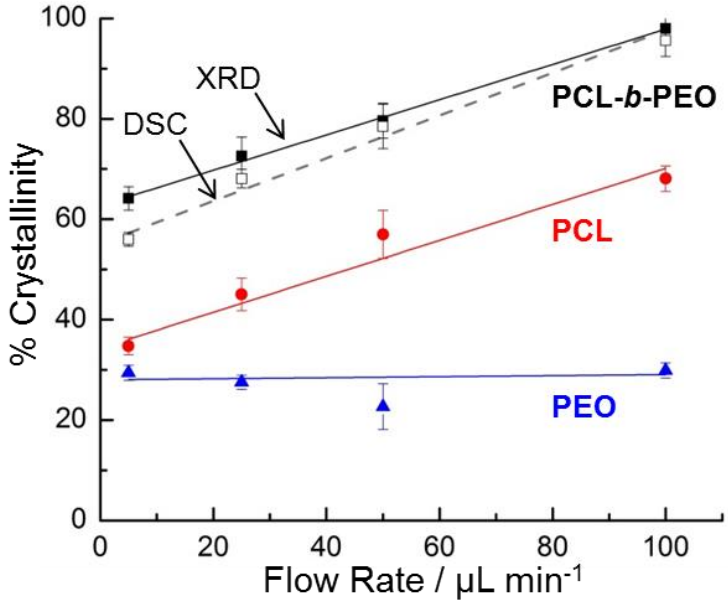

Figure 3. Percentages of crystallinity relative to the total copolymer mass for PCL-*b*-PEO nanoparticles formed on-chip at cwc + 10 wt % and various flow rates.

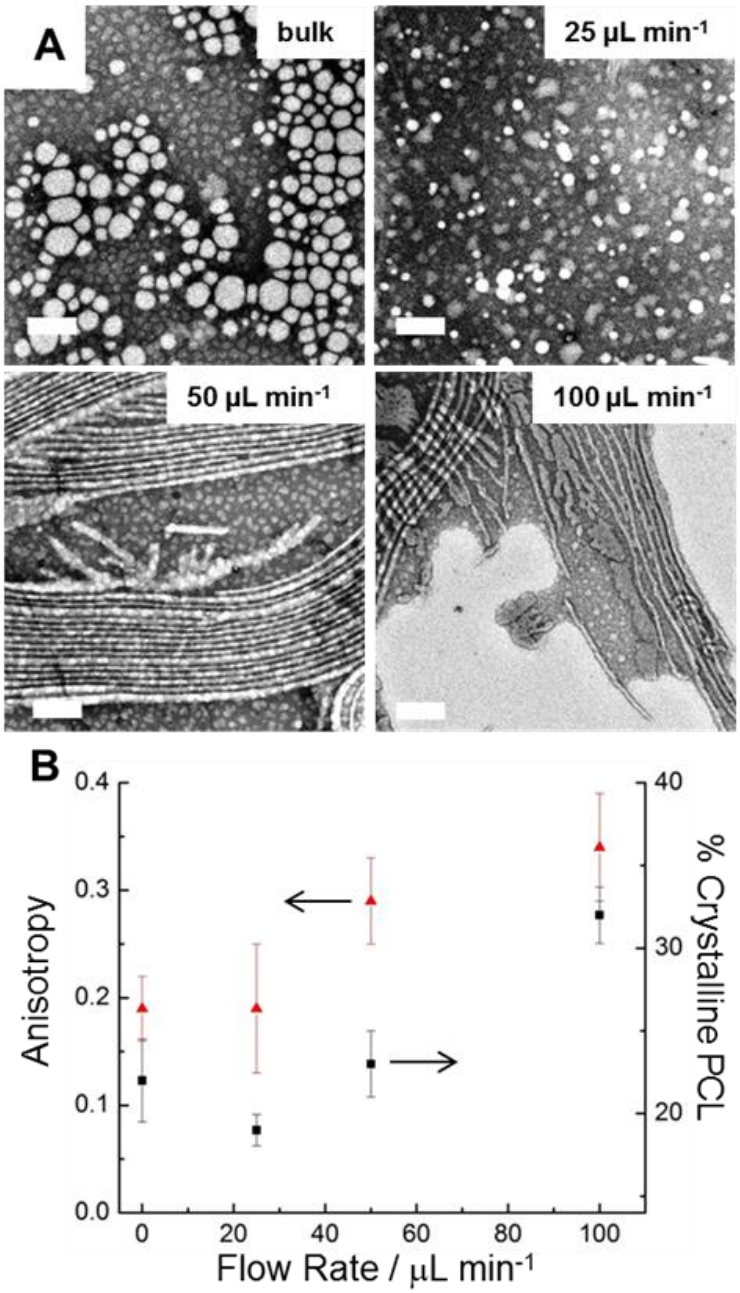

Figure 4. (A) TEM images of PAX-loaded nanoparticles formed on-chip at cwc + 5 wt % and various flow rates. Images were produced with negative staining and all scale bars are 200 nm. (B) Percentages of crystalline PCL (■) and fluorescence anisotropies of DPH probe (▲), revealing the core environments within the associated nanoparticles.

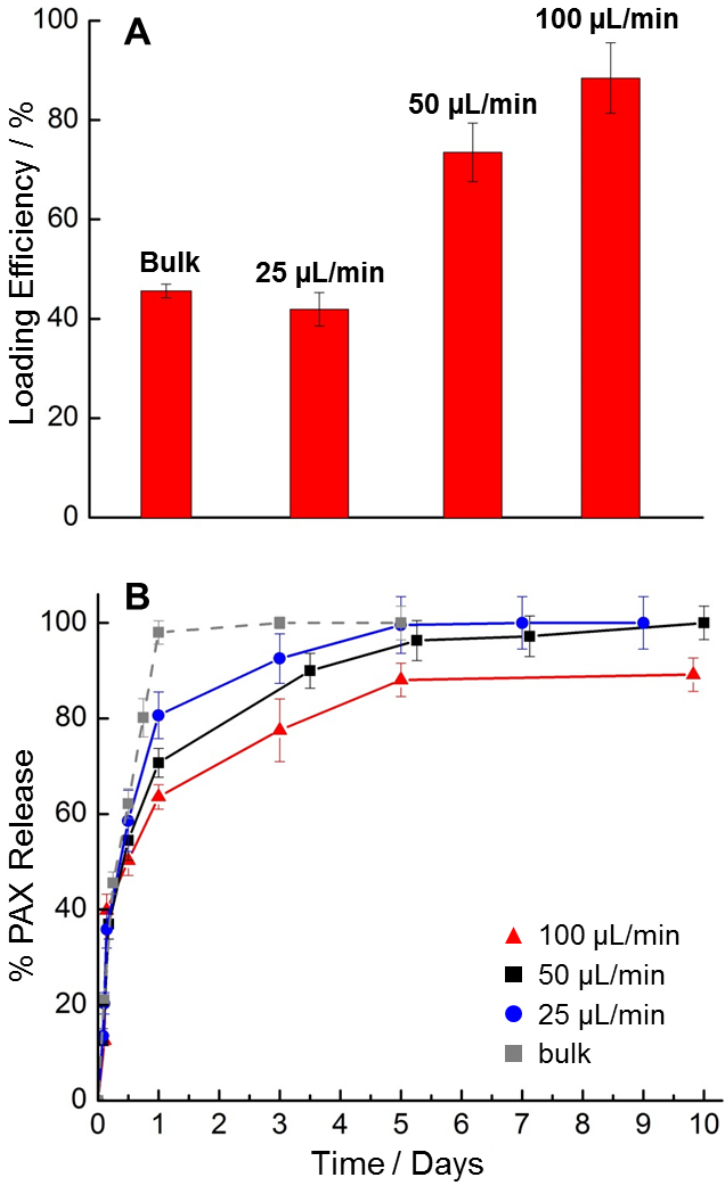

Figure 5. PAX loading efficiencies (A) and release kinetics (B) for PAX-loaded nanoparticles formed on-chip at cwc + 5 wt % and various flow rates, and a bulk-prepared control sample.

Acknowledgments

We are grateful to NSERC Canada for financial support and to Drs. Alex Leung (University of Victoria, UVic), David Sinton (University of Toronto), and Thomas Redelmeier (Northern Lipids Incorporation) for their contributions. We also acknowledge Dr. Patrick Nahirney and the UVic EM lab (Department of Biology) for the continued use of their TEM.

REFERENCES

[1] (a) Zhang, L.; Eisenberg, A. *Science* **1995**, *268*, 1728. (b) Zhang, L.; Eisenberg, A. *J. Am. Chem. Soc.* **1996**, *118*, 3168. (c) Mai, Y.; Eisenberg, A. *Chem. Soc. Rev.* **2012**, *41*, 5969. (d) Discher, B. M.; Won, Y.-Y.; Ege, D. S.; Lee, J. C.-M.; Bates, F. S.; Discher, D. E.; Hammer, D. A. *Science* **1999**, *284*, 1143. (e) Jain, S.; Bates, F. S. *Science* **2003**, *300*, 460. (f) Cui, H.; Chen, Z.; Zhong, S.; Wooley, K. L.; Pochan, D. J. *Science* **2007**, *317*, 647. (g) Wang, X. S.; Guerin, G.; Wang, H.; Wang, Y. S.; Manners, I.; Winnik, M. A. *Science* **2007**, *317*, 644. (h) Forster, S.; Plantenberg, T. *Angew. Chem., Int. Ed.* **2002**, *41*, 688. (i) Li, Z.; Kesselman, E.; Talmon, Y.; Hillmyer, M. A.; Lodge, T. P. *Science* **2004**, *306*, 98.

[2] (a) Allen, C.; Maysinger, D.; Eisenberg, *A. Coll. Surf. B: Biointerf.* **1999**, *16*, 3. (b) Discher, D. E.; Ortiz, V.; Srinivas, G.; Klein, M. L.; Kim, Y.; Christian, D.; Cai, S.; Photos, P.; Ahmed, F. *Prog. Polym. Sci.* **2007**, *32*, 838. (c) Tyrrell, Z. L.; Shen, Y.; Radosz, M. *Prog. Polym. Sci.* **2010**, *35*, 1128. (d) Parveen, S.; Misra, R.; Sahoo, S. K. *Nanomed.: NBM* **2012**, *8*, 147. (e) Gong, J.; Chen, M.; Zheng, Y.; Wang, S.; Wang, Y. *J. Control. Release* **2012**, *159*, 312. (f) Ahmad, Z.; Shah, A.; Siddiq, M.; Kraatz, H.-B. *RSC Adv.* **2014**, *4*, 17028. (g) Oltra, N. S.; Nair, P.; Discher, D. E. *Annu. Rev. Chem. Biomol. Eng.* **2014**, *5*, 281. (h) Yokoyama, M. *J. Drug Target.* **2014**, *22*, 576.

[3] Gonzalez, D.C.; Savariar, E. N.; Thayumanavan, S. *J. Am. Chem. Soc.* **2009**, *131*, 7708.

[4] (a) Torchilin, V. P. *Adv. Drug Delivery Rev.* **2002**, *54*, 235. (b) Nasongkla, N.; Bey, E.; Ren, J. M.; Ai, H.; Khemtong, C.; Guthi, J. S.; Chin, S. F.; D., S. A.; Boothman, D. A.; Gao, J. M. *Nano Lett.* **2006**, *6*, 2427. (c) Wu, W. C.; Chen, C. Y.; Tian, Y. Q.; Jang, S. H.; Hong, Y. N.; Liu, Y.; Hu, R. R.; Tang, B. Z.; Lee, Y. T.; Chen, C. T.; C., C. W.; Jen, A. K. Y. *Adv. Funct. Mater.* **2010**, *20*, 1413.

[5] (a) Wang, J. F.; Chen, Q. J.; Zhao, H.; Ming, T.; Wu, C. *J. Am. Chem. Soc.* **2009**, *131*, 16650. (b) Zhang, M.; Wang, M. F.; He, S.; Qian, J. S.; Saffari, A.; Lee, A.; Kumar, S.; Hassan, Y.; Guenther, A.; Scholes, G.; Winnik, M. A. *Macromolecules* **2010**, *43*, 5066.

[6] (a) Wang, C.-W.; Sinton, D.; Moffitt, M. G. *J. Amer. Chem Soc.* **2011**, *133*, 18853. (b) Wang, C.-W.; Bains, A.; Sinton, D.; Moffitt, M. G. *Langmuir*. **2012**, *28*, 15756. (c) Wang, C.-W.; Sinton, D.; Moffitt, M. G. *ACS Nano.* **2013**, *7*, 1424. (d) Wang, C.-W.; Bains, A.; Sinton, D.; Moffitt, M. G. *Langmuir.* **2013**, *29*, 8385.

[7] He, W.-N.; Xu, J.-T. *Prog. Polym. Sci.* **2012**, *37*, 1350.

[8] (a) Cai, S.; Vijayan, K.; Chen, D.; Lima, E. M.; Discher, D. E. *Pharmaceut. Res.* **2007**, *24*, 2099. (b) Geng, Y.; Dalhaimer, P.; Cai, S.; Tsai, R.; Tewari, M.; Minko. T.; Discher, D. E. *Nature Nanotech.* **2007**, *2*, 249. (c) Venkataraman, S.; Hedrick J. L.; Ong, Z. Y.; Yang, C.; Ee, P. L. R.; Hammond, P. T.; Yang, Y. Y. *Adv. Drug Deliv. Rev.* **2011**, *63*, 1228. (d) Oltra, N. S.; Swift, F.; Mahmud, A.; Rajagopal, K.; Lovede, S. M.; Discher, D. E. *J. Mater. Chem. B* **2013**, *1*, 5177.

[9] (a) Letchford, K.; Liggins, R.; Burt, H. *Eur. J. Pharm. Biopharm.* **2009**, *71*, 196. (b) Glover, A. L.; Nikles, S. M.; Nikles, J. A.; Brazel, C. F.; Nikles, D. E. *Langmuir* **2012**, *28*, 10653.

[10] (a) Karnik, R.; Gu, F.; Basto, P.; Cannizzaro, C.; Dean, L.; Kyei-Manu, W.; Langer, R.; Farokhzad, O. C. *Nano Lett.* **2008**, *8*, 2906. (b) Capretto, L.; Carugo, D.; Mazzitelli, S.; Nastruzzi, C.; Zhang, X. *Adv. Drug Deliv. Rev.* **2013**, *65*, 1496.

[11] He, W.-N.; Xu, J.-T.; Du, B.-Y.; Fan, Z.-Q. *Macromolecules* **2012**, *45*, 9768.

[12] (a) Du, Z.-X.; Xu, J.-T. Xu; Fan, Z.-Q. *Macromol. Rapid Commun.* **2008**, *29*, 467. (b) Rizis, G.; van de Ven, Th. G. M.; Eisenberg, A. *Soft Matter* **2014**, *10*, 2825.

[13] Lamberti, G. *Chem. Soc. Rev.* **2014**, *43*, 2240.

[14] Geng, Y.; Discher, D. E. *J. Amer. Chem. Soc.* **2005**, *127*, 12780.

Table of Contents Entry

Hierarchical semicrystalline block copolymer nanoparticles are produced in a segmented gas-liquid microfluidic reactor with top-down control of multiscale structural features, including nanoparticle morphologies, sizes, and internal crystallinities. Control of multiscale structure on disparate length scales by a single control variable (flow rate) enables tailoring of drug delivery nanoparticle function including release rates.

Aman Bains, Yimeng Cao, Matthew G. Moffitt*

Multiscale Control of Hierarchical Structure in Crystalline Block Copolymer Nanoparticles using Microfluidics